ChemPubSoc Europe

DOI: 10.1002/open.201900111

Open Access ChemistryOPEN Full Papers

Synthesis, Structural Characterization and Photodecarbonylation Study of a Dicarbonyl Ruthenium (II)-Bisquinoline Complex

Manja Kubeil,*[a] Tanmaya Joshi,[a] Bayden R. Wood,[b] and Holger Stephan*[a]

A photoactivatable ruthenium(II) carbonyl complex *mer,cis*-[Ru(II)Cl(BisQ)$(CO)_2$]PF_6 **2** was prepared using a tridentate bisquinoline ligand (BisQ = (2,6-diquinolin-2-yl)pyridin). Compound **2** was thoroughly characterized by standard analytical methods and single crystal X-ray diffraction. The crystal structure of the complex cation reveals a distorted octahedral geometry. The decarbonylation upon exposure to 350 and 420 nm light was monitored by UV/VIS absorbance and Fourier transform infrared spectroscopies in acetonitrile and 1% (v/v) DMSO in water, respectively. The kinetic of the photodecarbonylation has been elucidated by multivariate curve resolution alternating least-squares analysis. The stepwise decarbonylation follows a serial mechanism. The first decarbonylation occurs very quickly whereas the second decarbonylation step proceeds more slowly. Moreover, the second rate constant is lower in 1% (v/v) DMSO in water than in acetonitrile. In comparison to 350 nm irradiation, exposure to 420 nm light in acetonitrile results in a lower second rate constant.

1. Introduction

Carbon monoxide (CO)-based therapy represents an exciting new frontier in biomedical research.[1] A pre-condition for successfully achieving the therapeutic benefits from the otherwise toxic CO is the ability to deliver it in controllable dosage, at specific targets.[1b,c,h,2] CO releasing molecules (CORMs) offer the unique possibility of exerting dosage control by first allowing the storage of CO in solid form, and then releasing it only in response to an endogenous or exogenous trigger.[1a,c,e,2–3] In previous works, decarbonylation from CORMs has been triggered by photo-irradiation (photoCORMs), enzymes, pH and thermal changes as well as by ligand exchange reactions.[1c,d,g,2a,3–4] Of these methods, light-triggered decarbonylation is particularly attractive as it offers greater spatial-temporal control.[1f,3–,4c,5] In this regard, several organic and inorganic photoCORMs have been identified.[1e,f, 3–,4c,6] Transition metal carbonyls have featured the most in such studies.[1e,f,3–,4c,6a] This is not at all surprising considering the vastly rich photochemistry of metal carbonyl compounds. A plethora of Mn, Fe, Cr, Re, and W complexes, which contain one or more photolabile M–CO bonds, have been evaluated for their aqueous solubility, stability, cellular toxicity and photodecarbonylation characteristics.[1f,g,4c,5–6,7] These studies have concluded that it is indeed possible to tune the CO releasing ability of such scaffolds by varying the ancillary ligand(s) around the metal center.

More recently, increasing attention has been given to Ru(II)-based photoCORMs. A number of research groups have shown that the Ru(II) dicarbonyl complexes can undergo photoinduced decarbonylation with relatively short half-lives.[8] Using a combination of spectroscopic techniques, theoretical calculations and multi-curve resolution alternating least-squares (MCR-ALS) analysis, we have also demonstrated that the rate of decarbonylation is solvent dependent.[8f] Additionally, the feasibility to chemically link the Ru(II)-based photoCORMs to delivery vectors without compromising on their CO-releasing properties has also been demonstrated.[1d,8a,9] This offers interesting possibilities regarding the development of Ru(II) photoCORMs as site-directed therapeutics.

We have now extended our ongoing investigations on Ru(II) photoCORMs to include π-electron rich quinoline-based systems to overcome the poor photochemistry of terpyridine-based structures.[10] Different strategies have been reported to shift the absorption band to the visible region by extending the π-system, altering the position of the nitrogen in the quinoline ring or adding electron-donating groups.[11] In this article, we report the synthesis, characterization and photodecarbonylation study of a new Ru(II) dicarbonyl complex featuring a tridentate bisquinoline ligand (Scheme 1). In addition to determining the crystal structure of the prepared Ru(II) complex, we have studied its photdecarbonylation behavior using electronic absorption, Fourier transform infrared (FTIR) and NMR spectroscopy as well as MCR-ALS to gain some insight into the effect of the introduced bisquinoline-type π system on decarbonylation activity.

[a] *Dr. M. Kubeil, Dr. T. Joshi, Dr. H. Stephan*
Institute of Radiopharmaceutical Cancer Research
Helmholtz – Zentrum Dresden – Rossendorf
Bautzner Landstrasse 400, 01328 Dresden, Germany
E-mail: m.kubeil@hzdr.de
h.stephan@hzdr.de
[b] *Prof. B. R. Wood*
School of Chemistry and Centre for Biospectroscopy
Monash University
Clayton, Victoria 3800, Australia

Supporting information for this article is available on the WWW under https://doi.org/10.1002/open.201900111

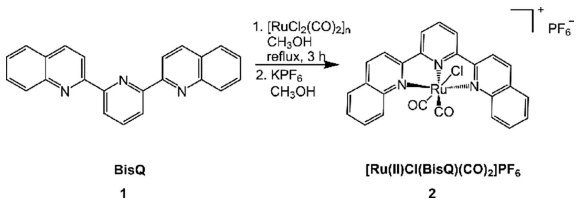

Scheme 1. Synthesis of *mer,cis*-[Ru(II)Cl(BisQ)$(CO)_2$]PF_6 **2**.

2. Results and Discussion

2.1. Synthesis and Characterization

The bisquinoline ligand BisQ **1** was synthesized by double Friedländer condensation of 2,6-acetylpyridine with *ortho*-substituted nitrobenzaldehyde in a one-pot reaction.[12] The Ru(II) complex was prepared by refluxing the key precursor $[RuCl_2(CO)_2]_n$[13] with **1** in methanol under inert atmosphere and exclusion of light to afford the pure *mer,cis*-[Ru(II)Cl(BisQ)$(CO)_2$]Cl **2** in moderate yield (51%) (Scheme 1). The chloride counteranion was replaced with a weakly coordinating hexafluorophosphate (PF_6^-) anion[14] by adding saturated KPF_6 solution in methanol to yield the complex as a PF_6^- salt. Complex **2** has theoretically two possible stereoisomers (*cis*-(CO) and *trans*-(CO)). The latter one is thermodynamically unfavorable and may not exist.[15] Therefore, only the *mer,cis*-(CO) isomer was isolated (confirmed by X-ray crystallography, as discussed later).

The complex was fully characterized by $^1H/^{13}C$, ^1H-^1H COSY NMR, ESI-MS, UV/VIS, FTIR, elemental and X-ray crystal structure analysis. The $^1H/^{13}C$ NMR in acetonitrile-d3 and DMSO-d6, ^1H-^1H COSY NMR, ESI-MS, IR and UV/VIS data of the complex are collected in Supporting Information (Figures S1–S7). Coordination of the ligand to the diamagnetic ruthenium(II) results in five signals, some of which are due to overlapping resonances, in the aromatic region with a slight up-field shift compared to the non-coordinated ligand in the ^1H NMR spectrum (Figure S1). The assignment of the aromatic protons was done by ^1H-^1H COSY NMR in acetonitrile-d3 (Figure S2). The two characteristic ^{13}CO signals in the ^{13}C NMR spectrum are observed at 201.0 and 187.8 ppm in acetonitrile-d3 (Figure S1) and at 195.5 and 187.0 ppm in DMSO-d6 (Figure S4).

The FTIR spectrum of the ruthenium(II) carbonyl complex (Figure S6) shows two strong carbonyl CO vibrations in the expected region from 2100–1900 cm^{-1}. The symmetrical stretching mode is assigned to higher (2075 cm^{-1}) and the antisymmetrical one to lower energy (2006 cm^{-1}).

The UV/VIS absorption spectrum of complex **2** was recorded in acetonitrile and 1% (v/v) DMSO in water (Table 1, Figure S7). In acetonitrile, the ruthenium complex displays four main transitions and a shoulder at ~275 nm; two bands below and two above 350 nm. Interestingly, the electronic spectrum of complex **2** in 1% (v/v) DMSO in water is similar to that in acetonitrile, except that the shoulder at ~275 nm has diminished and five rather than four distinct bands can be observed, three below 350 nm and two above. The extinction coefficients are quite intense (Figure S7, Table 1), but similar to the reported Ru(II)complexes bearing quinoline ligands.[10,16] The transitions can be assigned to π-π* (ligand-based absorption) and MLCT/LLCT.[16] In comparison, only two distinct bands have been reported in literature for the Ru(II) dicarbonyl terpyridine complex **4** (Scheme 2) in DMSO, with the absorption maxima

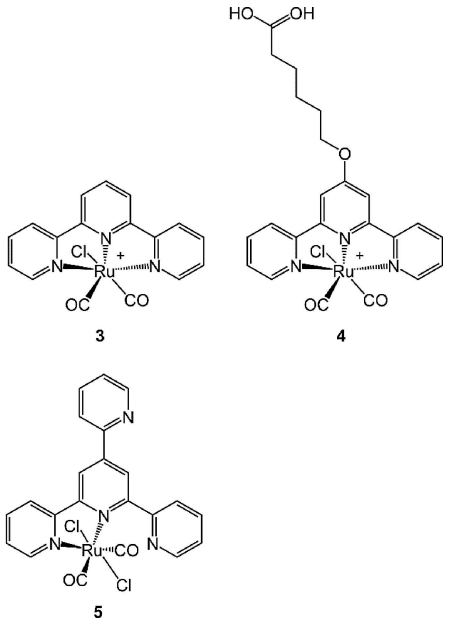

Scheme 2. Structures of reported Ru(II) carbonyl complexes with terpyridine scaffolds.

observed below 350 nm.[8a] Thus, the extension of the π-system from having terpyridyl to quinolyl ligand in the coordination sphere results in a bathochromic shift.

A single pale, light-green crystal of the monocationic complex **2** suitable for X-ray diffraction analysis was obtained by slow diffusion of chloroform into the acetone solution, over two weeks. The molecular structure of the cationic complex **2** is shown in Figure 1 and selected bond length and angles are listed in Table S1. The crystallographic parameters are shown in Supporting Information (Tables S1–S6). The ruthenium(II) bisquinoline chloro dicarbonyl cation exists as the *mer,cis*-(CO)-

Table 1. Absorption maxima and molar extinction coefficients for complex **2** in acetonitrile and 1% (v/v) DMSO in H_2O at room temperature.

solvent	$\varepsilon_{\lambda max}$ [$M^{-1}cm^{-1}$] (λ_{max} [nm])	$\varepsilon_{\lambda max}$ [$M^{-1}cm^{-1}$] (λ_{max} [nm])	$\varepsilon_{\lambda max}$ [$M^{-1}cm^{-1}$] (λ_{max} [nm])	$\varepsilon_{\lambda max}$ [$M^{-1}cm^{-1}$] (λ_{max} [nm])
acetonitrile	40000 ± 700 (252)	16000 ± 400 (319)	16700 ± 200 (355)	26700 ± 200 (375)
1% (v/v) DMSO in water	36200 ± 900 (250) 36600 ± 900 (273)	14500 ± 300 (314)	16500 ± 400 (360)	24500 ± 600 (377)

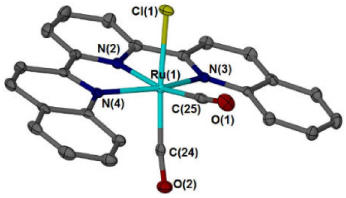

Figure 1. Molecular structure of the cationic unit of **2**.

isomer and adopts a distorted octahedral geometry, which is a result of the bite angle of the tridentate ligand (N(4)–Ru–N(3)) at 155.85(9)°. The Ru–N(3) and Ru–N(4) bond lengths are slightly elongated with 2.130(2) Å and 2.127(2) Å, while the Ru–N(2) bond length is compressed at 2.017(2) Å. Moreover, the axial Ru-CO bond length (CO *trans* to Cl) is shorter (1.887(3) Å) than that of the equatorial Ru-CO bond (CO *cis* to Cl) with 1.908(3) Å. For comparison, the X-ray crystal structure of a similar ruthenium(II) dicarbonyl compound with a tridentate terpyridyl ligand (see structure **3**, Scheme 2) revealed a slightly different situation.[17] The X-ray data of the terpyridyl complex show that the Ru–N(3) and Ru–N(4) bond lengths are shorter with 2.092(2) Å and 2.097(2) Å, while the Ru–N(2) bond length is similar at 2.016(2). Interestingly, the reported axial Ru-CO distance (1.873(3) Å) is shorter than in complex **2** whereas the equatorial Ru-CO bond length is similar (1.912(3) Å). This may influence the decarbonylation properties and hence the kinetics. The longer the Ru-CO bond length, the faster might be the decarbonylation step and the less energy is needed for excitation. Furthermore, the Ru–Cl bond distance in **2** is slightly longer than in **3** with 2.3997(7) Å vs. 2.3917(7) Å.

2.2. Light-Induced Decarbonylation Monitored by UV/Vis, FTIR and ^{13}C NMR Spectroscopy

UV/Vis absorption spectra of complex **2** was measured over time, in both acetonitrile and 1% (v/v) DMSO in water (Figure 2), to monitor the photolysis at exposure to 350 nm irradiation. Additionally, photolysis of **2** was examined at 420 nm in acetonitrile. Due to similar absorption profiles of the species formed upon irradiation at 350 and 420 nm, just the changes in the absorption spectrum upon irradiation at 350 nm are depicted in Figure 2 (for 420 nm irradiation cf. Figure S8). Prior to photolysis experiments, the complex was stored in the dark and kept under air in the respective solvent. The sample revealed no spectral changes over a period of 21 h (Figure S7). Furthermore, the experimental setup does not allow recording of spectra with less than 10 s irradiation. Upon irradiation at 350 and 420 nm in acetonitrile, the absorption spectra of **2** showed five bands of increasing intensity (λ_{max} ~255, 316, 348, 430–750) within 3.5 h (Table 1 for comparison with non-irradiated species). Only two new broad bands appeared in the region between 430 and 750 nm. The band at 348 nm (non-irradiated species at λ_{max} = 355 nm) underwent a slight hypsochromic shift (~7 nm). Whereas the band at 375 nm decreased in intensity and the shoulder at ~275 nm diminished within

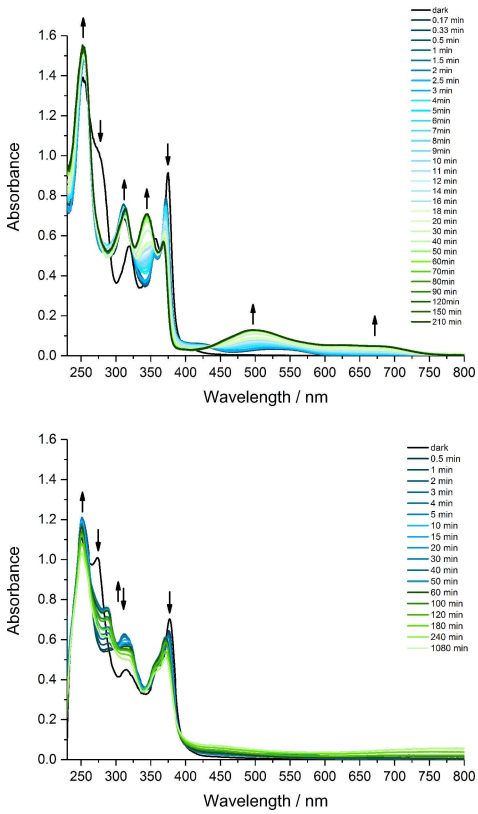

Figure 2. UV/VIS absorption spectra of complex **2** in acetonitrile (top, 36 μM) and in 1% (v/v) DMSO in water (bottom, 30 μM) after different periods of exposure to 350 nm of irradiation (E_v ~2.5 mW/cm^2) at room temperature.

time. No more significant changes in the spectrum occurred after 210 min.

Photolysis experiments at 350 nm were also performed in 1% (v/v) DMSO in water in particular to test the complex under aqueous conditions with regard to in vitro experiments (Figure 2 bottom). The complex showed fewer changes in the absorption profile compared to the photolysis experiments in acetonitrile. The band at 273 nm diminished upon brief exposure to UV light (>10 s) and a new one formed at ~290 nm. The UV bands at 250 and ~377 nm decreased in intensity and the latter one underwent a slight hypochromic shift (~5 nm), whereas the band at 314 nm increased in intensity. No more significant changes in the spectrum occurred after 4 h.

To elucidate the mechanism and kinetics of photolysis, the UV/VIS spectra were analyzed by MCR-ALS analysis, as described previously[8f] and in the experimental section. Kinetic models were determined for the observed changes in the spectra in both solvents. Two consecutive steps and three individual species (A, P1 and P2; Scheme S1) were calculated in acetonitrile at 350 and 420 nm (Table 2). The first reaction occurs very quickly, i.e., the absorption spectra change drastically upon the initial irradiation. Only two spectra were available for the fit and, consequently, the rate constants k_1 are considered lower limits only. The second rate constant (k_2) for the photoreaction at 350 nm is a bit higher than k_2 at 420 nm.

Table 2. Fitted rate constants and half-lives of complex 2 in acetonitrile and 1% (v/v) DMSO in H_2O exposed to 350 and 420 nm at room temperature.

	Acetonitrile at 350 nm	Acetonitrile at 420 nm	1% (v/v) DMSO in water at 350 nm
k_1 [min^{-1}] (τ [min])	~14 (~0.2)	~14 (~0.2)	3.05 ± 0.02 (0.23)
k_2 [min^{-1}] (τ [min])	0.0478 ± 0.0004 (~14)	0.03 ± 0.01 (~26)	0.13 ± 0.005 (5)
k_3 [min^{-1}] (τ [min])	–	–	0.005 ± 0.0002 (139)

In 1% (v/v) DMSO in water three consecutive steps and four individual compounds (Table 2 and Scheme S1) were fitted by MCR-ALS.

The fitted spectra and concentration profiles for complex **2** and their photoproducts are shown in Supporting Information (Figures S9 and S10). It should be noted that although the rate constant results from an exponential decay as function of concentration, it is not a unimolar rate constant for the associated photoreaction as such (see Eqs. 1 to 4). It is rather a result of the reaction conditions of this photochemical reaction[1g,18], which is not defined as the classical rate constant. Thus, it should not be misunderstood as a common rate constant.

The rate of a photochemical reaction[18a] is best described as:

$$-\frac{dc}{dt}=\varphi \cdot I_{abs} \quad (1)$$

where c represents the concentration, t time, Φ the quantum yield and I_{abs} is the absorbed light intensity.

Inserting the definition of the absorbance $A(\lambda)$ gives:

$$-\frac{dc}{dt}=\varphi \cdot I_0(1-10^{-A(\lambda)}) \quad (2)$$

where I_0 is the incident light intensity.

When $A(\lambda) \ll 1$, the right hand side can be approximated by using Taylor series ($(1-10^{-A(\lambda)}) \cong 2.3\ A(\lambda)$) and the absorbance can be replaced using the Lambert-Beer-Law:

$$-\frac{dc}{dt} \approx \varphi \cdot I_0 \cdot 2.3 \cdot A(\lambda) = \varphi \cdot I_0 \cdot 2.3 \cdot \varepsilon \cdot c \cdot d \quad (3)$$

where ε is the molar extinction coefficient ($M^{-1}cm^{-1}$) and d is the pathlength in a cell (cm).

As a consequence, the rate constant resembles a first order kinetics:

$$-\frac{dc}{dt}=k \cdot c \quad (4)$$

with $k = \varphi \cdot I_0 \cdot 2.3 \cdot \varepsilon \cdot d$

However, for identical measurement conditions and similar extinction coefficients (Table 1), the determined values of k_n are a good representation of the quantum yield and therefore, can be meaningfully discussed instead.

Moreover, the UV-light-induced decarbonylation characteristics of the complex in acetonitrile was assessed by FTIR spectroscopy. FTIR spectra of the irradiated complex were recorded after the deposition of an aliquot of an irradiated complex solution onto a silicon ATR accessory and drying it with N_2 gas. Spectral changes (Figure 3) in the characteristic CO

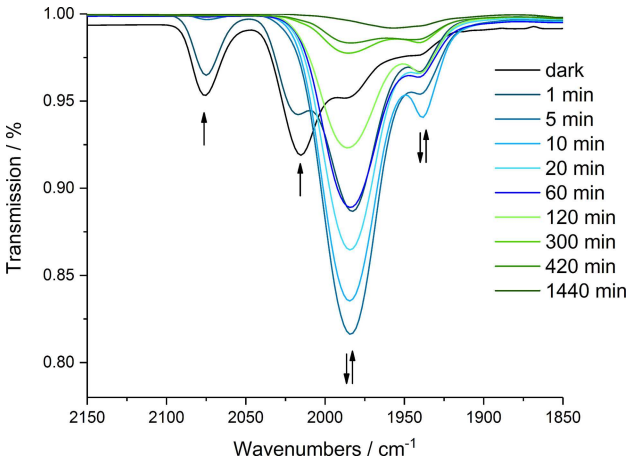

Figure 3. FTIR spectra (2150–1900 cm^{-1}) of complex **2** after different periods of exposure to 350 nm of irradiation in acetonitrile at room temperature.

region (2150–1850 cm^{-1}) were observed upon irradiation of **2** at 350 nm. The intensities of the two CO bands associated with the starting complex diminished over a certain period upon exposure to UV light. One intense new stretching vibration at 1984 cm^{-1} appeared after 5 min. We assume that the monocarbonyl species $[Ru(II)Cl(BisQ)(solvent)CO]^+$ was generated[8f] (see FTIR spectrum after 5 min, Figure 3). The intensity of the CO band associated with the monocarbonyl species progressively diminished with time, indicating the complete decarbonylation within the time course of the experiments.

The complete photolysis profile of complex **2** was also monitored by ^{13}C NMR spectroscopy. As shown in Figure S4, the typical ^{13}CO signals at $\delta = 195.5$ and 187.0 ppm completely disappear after exposure to 350 nm irradiation for 4 h in a DMSO-d6 solution.^{13}C NMR was not possible to measure in deuterated acetonitrile due to the precipitation of the species formed upon irradiation. Nonetheless, the complete decarbonylation of complex **2** is supported by the FTIR spectroscopy measurements in acetonitrile and the ^{13}C NMR data for the irradiated sample in DMSO-d6 (Figures 3 and S4).

In summary, the photoreaction involves a stepwise decarbonylation. The first decarbonylation occurs very quickly, which can be observed by the dramatic change of the absorption profile even upon brief (> 10 s) UV-light exposure. The second decarbonylation step ($k_2 \gg k_1$) proceeds much slower and k_2 is

even lower when light irradiation is performed at 420 nm compared to 350 nm. In general, the absorption profile of the photodecarbonylation is less pronounced in 1% (v/v) DMSO in water and process seems to be slower than in acetonitrile. That the dicarbonyl Ru(II) complex **2**, where the bisquinoline ligand coordinates in a meridonal tridentate mode, is capable of undergoing complete decarbonylation can be confirmed by FTIR and ^{13}C NMR spectroscopy. In contrast, terpyridyl ligand in the reported - dicarbonyl Ru(II)CORM complex **5** (Scheme 2)[16] initially exhibits a bidentate coordination mode, which changes into the meridonal tridentate only after the exposure of the complex to UV light and its subsequent monodecarbonylation.

3. Conclusions

The synthesized ruthenium(II) dicarbonyl complex based on tridentate bisquinoline ligand exhibits beneficial electronic properties, which manifest in a complete decarbonylation after photoactivation at 350 nm and 420 nm, as confirmed by FTIR and ^{13}C NMR spectroscopy. Furthermore, the conjugated π-system can be altered and extended, respectively, to actually push the absorption range into the visible spectrum. Anchoring ancillary groups to the skeleton of the bisquinoline ligand gives the possibility to attach biomolecules for targeted therapy.

Experimental Section

All reactions were performed under nitrogen atmosphere using standard Schlenk techniques and assemblies were protected from light if necessary by wrapping them with aluminium foil. Analytical-grade solvents were degassed by purging with nitrogen for at least 30 min before use if necessary. All solvents were purchased from Sigma-Aldrich or BioScientific and used as received. Ruthenium trichloride hydrate was purchased from Strem Chemicals (#44-5880). 2-Nitrobenzaldehyde (#A11501) was purchased from Alfa Aesar. Iron powder (#12310) and 2,6-Diacetylpyridine (#D8801) were bought from Sigma-Aldrich. Formic acid, 99% was obtained from Fluka. All solvents were purchased from commercial sources (Sigma–Aldrich, Fluka, VWR, Fisher Scientific) without further purification. A Direct-Q 3 UV water purification system from Millipore (Merck KGaA) was applied to produce ultrapure water. The resistivity of the ultrapure water was 18.2 MΩ/cm. Ligand BisQ 2,6-di(quinolin-2yl)pyridine **1** and the polymer $[RuCl_2(CO)_2]_n$, were synthesized according to literature.[12–13] All characterization data were in agreement with literature reports.

NMR Spectra were recorded at 298 K on an Agilent DD2-400 MHz NMR or an Agilent DD2-600 MHz NMR spectrometer with ProbeOne Chemical shifts δ are reported in parts per million (ppm) relative to tetramethylsilane. Coupling constants J are given in Hertz. Abbreviations for the peak multiplicities are as follows: s (singlet), d (doublet), dd (doublet of doublets), ddd (doublet of doublets of doublets), t (triplet), and m (multiplet).

UV/VIS Spectra were recorded on a Cary 300 spectrophotometer (Agilent Technologies).

Elemental Analysis (C, H, N) was carried out at the Campbell Microanalytical Laboratory, University of Otago, New Zealand. Electrospray ionization mass spectrometry (ESI-MS) was carried out on an Agilent 6120 series Quadrupole LC/MS system.

ATR-FTIR Spectra were acquired on a Bruker model Equinox 55 FT-IR spectrometer fitted with a N_2-cooled mercury-cadmium-telluride (MCT) detector. A Specac golden gate diamond or a Harrick silicon multiple reflection ATR accessory was used for spectral acquisition. The silicon ATR accessory was used to acquire spectra of samples in solvated state. For this purpose, 4 μL acetonitrile solutions of complex (1 mg/mL) were deposited on the silicon ATR followed by evaporation (10 min) under a gentle N_2 flow resulting in a thin film of compound for direct measurement. The spectra were acquired with OPUS software 6.0. ATR spectra were collected in the wavenumber range between 4000 and 400 cm^{-1} at a spectral resolution of 4 cm^{-1}, and 50 interferograms were co-added. Preprocessing of the spectral data was performed with the OPUS 7.2 software. ATR-FTIR spectra were baseline-corrected using concave rubberband correction.

X-Ray Crystallography. Intensity data for green crystals of **2** ($0.75\times0.25\times0.05$ mm^3) were measured at 123 K on a Bruker Apex II CCD fitted with graphite monochromated Mo Kα radiation (0.71073 Å). The data was collected to a maximum 2θ value of 50° and processed using the Bruker Apex II software package. Crystal parameters and details of the data collection are summarized in Table S1 in the Supporting Information. The structure was solved by direct method and expanded using standard Fourier routines in the SHELX-97.[19] All hydrogen atoms were placed in idealized positions. A mixture of chloroform and acetone molecule of crystallization was located on the Fourier difference map and refined anisotropically, fixing their respective site occupancy factors as 50%. All non-hydrogen atoms were refined anisotropically.

Photolysis Experiments were conducted using a Rayonet Photoreactor (RPR-200 model) fitted with two Rayonet lamps with an emission wavelength centered at 350 nm (full width at half maximum = 45 nm; $E_v \approx 2.5$ mW cm^{-2}) and 420 nm (full width at half maximum = 30 nm). A 1 cm quartz fluorescence cuvette (3 mL) was used as the reaction vessel. The power density was measured using a power meter with a built in photodiode sensor (PM200 series) from Thorlabs. The rate of decarbonylation upon exposure of UV light was measured by recording the UV/VIS absorption spectra (200–800 nm) of complex **2** in acetonitrile or 1% (v/v) DMSO in H_2O at certain time intervals. All experiments were performed in duplicate.

Multivariate Curve-Fitting Analysis. UV/Vis absorbance spectra for all time points were imported into a Matlab matrix. The Matlab Toolbox MCR-ALS 2.0[20] was used to estimate the number of components by the inbuilt singular value decomposition algorithm and to extract the spectrum and transient concentration development of each component using a MCR-ALS algorithm.[21] The number of components was determined from the number of eigenvalues ≥1 and confirmed later by manual variation of the number of components, available time points, and an adapted kinetic model constraint. The initial estimates of the spectra were determined by means of the purest variable detection method. The following constraints were set for the ALS optimization: (i) non-negativity for all species concentrations and spectra via non-negative least squares (nnls) and (ii) a kinetic constraint to correlate the different species via a consecutive kinetic model, A→P1…→Pi with rate constant k_i (Scheme S1), with the predefined number of species. At the beginning, only one species exists, and therefore only the initial concentration (of species A) was different from zero and set to 35 μM. Estimates for the reaction rate constants were $k_1 = 1$ min^{-1}, $k_2 = 0.1$ min^{-1}, and $k_3 = 0.01$ min^{-1}. No normalization of any spectrum was applied, and convergence was typically achieved in less than 100 iterations with a convergence limit of 10^{-3}. Half-life times have been calculated by (pseudo) first order in comparison to other reported ones, although in general the concept of a kinetic

order of a photoreaction is not appropriate (for detailed explanation see [1g]).

Chloro-*cis*-dicarbonyl-*mer*-((2,6-diquinolin-2-yl)pyridin)ruthenium (II) hexafluorophosphate [RuCl(BisQ)(CO)$_2$]PF$_6$ (2). A suspension of **1** (0.5 mmol) in methanol (20 mL) was refluxed for 10 min and then $[RuCl_2(CO)_2]_n$ (114 mg) was added. The suspension was refluxed for 1.5 h under nitrogen atmosphere and exclusion of light. After cooling to room temperature, the green solution was filtered and the solvent was removed in vacuo. The residue was dissolved in a minimum amount of chloroform, then methanol was added until precipitation occurred and stored in the fridge to allow further precipitation. The precipitate was filtered and dried in a desiccator to yield **2(Cl)** (142 mg, 51 %) as a green solid. ^{1}H NMR (400 MHz, DMSO-d6, TMS): δ 9.17 (d, 2H, ^{3}J = 8.2, H$_{arom.}$), 9.13 (d, 2H, ^{3}J = 8.4, H$_{arom.}$), 9.00 (d, 2H, ^{3}J = 8.7 Hz, H$_{arom.}$), 8.85-8.74 (m, 3H, H$_{arom}$), 8.36 (d, 2H, ^{3}J = 8.2, H$_{arom.}$), 8.26 (ddd, 2H, ^{3}J = 8.6, ^{3}J = 6.9, ^{2}J = 1.4, H$_{arom.}$) 8.02 (t, 2H, ^{3}J = 7.6, H$_{arom.}$) ppm. ^{13}C NMR (101 MHz, DMSO-d6, TMS): δ = 195.5 (CO), 187.0 (CO), 159.9, 155.9, 148.0, 142.8, 142.5, 134.1, 132.1, 130.0, 128.4, 126.5, 121.2, 119.9 (C$_{arom.}$) ppm. Counter anion exchange: The complex **2(Cl)** (65 mg, 0.12 mmol) was dissolved in 7 mL methanol and the filtered to remove the residue. The filtrate was treated with 3 mL saturated KPF_6 solution and stored in the fridge for 1 h. The precipitate was collected by filtration, washed several times with water and dried in a desiccator overnight to yield complex **2** (55 mg, 82 %) as a light green solid. ^{1}H NMR (400 MHz, CD_3CN, TMS): δ 8.89 (d, 2H, ^{3}J = 8.6 Hz, H$_{arom.}$), 8.78 (d, 2H, ^{3}J = 8.1 Hz, H$_{arom.}$), 8.66–8.60 (m, 5H, H$_{arom}$), 8.25–8.20 (m, 4H, H$_{arom.}$), 7.99–7.95 (m, 2H, H$_{arom.}$) ppm. ^{13}C NMR (101 MHz, CD_3CN, TMS): δ = 201.0 (CO), 187.8 (CO), 161.1, 157.5, 150.1, 144.3, 143.8, 135.7, 131.7, 131.5, 129.8, 127.6, 122.2 (C$_{arom.}$) ppm. UV/VIS (CH_3CN): λ_{max} (ε) = 375 (26700), 355 (16799), 319 (16000), 251 nm (40000 $M^{-1}cm^{-1}$); IR (silicon, ATR): 2075, 2006 cm^{-1} (CO); MS (ESI$^+$): m/z (%): 552 (100) $[M-2CO+2CH_3CN-PF_6]^+$, 539 (55) $[M-CO+CH_3CN-PF_6]^+$; elemental analysis calcd. (%) for $C_{25}H_{16}ClF_6N_3O_{2.5}PRu$: C 44.16, H 2.37, N 6.18 found: C 43.90 H 2.33, N 6.17.

Acknowledgements

The author thanks Dr habil. C. Mamat for support with 2D NMR assignment. Dr C. Kubeil is greatly acknowledged for the fruitful discussions about the photoreactions and their kinetic orders and rate constants. MK was supported by a Marie Curie International Outgoing Fellowship from the European Union's Seventh Framework Programme for research, technological development and demonstration under grant agreement no. 627113.

Conflict of Interest

The authors declare no conflict of interest.

Keywords: photoCORM · ruthenium · tridentate ligand · UV/VIS and FTIR · photodecarbonylation

[1] a) B. E. Mann, *Organometallics* **2012**, *31*, 5728–5735; b) I. C. Winburn, K. Gunatunga, R. D. McKernan, R. J. Walker, I. A. Sammut, J. C. Harrison, *Basic Clin. Pharmacol. Toxicol.* **2012**, *111*, 31–41; c) S. García-Gallego, G. J. L. Bernardes, *Angew. Chem. Int. Ed.* **2014**, *53*, 9712–9721; *Angew. Chem.* **2014**, *126*, 9868–9877; d) A. C. Kautz, P. C. Kunz, C. Janiak, *Dalton Trans.* **2016**, *45*, 18045–18063; e) M. Kourti, W. G. Jiang, J. Cai, *Oxid. Med. Cell. Longev.* **2017**, *2017*, 9326454–9326454; f) R. D. Rimmer, A. E. Pierri, P. C. Ford, *Coord. Chem. Rev.* **2012**, *256*, 1509–1519; g) P. C. Ford, *Coord. Chem. Rev.* **2018**, *376*, 548–564; h) R. Motterlini, L. E. Otterbein, *Nat. Rev. Drug Discovery* **2010**, *9*, 728.

[2] a) S. H. Heinemann, T. Hoshi, M. Westerhausen, A. Schiller, *Chem. Commun.* **2014**, *50*, 3644–3660; b) X. Ji, K. Damera, Y. Zheng, B. Yu, L. E. Otterbein, B. Wang, *J. Pharm. Sci.* **2016**, *105*, 406–416.

[3] U. Schatzschneider, *Br. J. Pharmacol.* **2015**, *172*, 1638–1650.

[4] a) U. Schatzschneider, *Inorg. Chim. Acta* **2011**, *374*, 19–23; b) P. C. Kunz, H. Meyer, J. Barthel, S. Sollazzo, A. M. Schmidt, C. Janiak, *Chem. Commun.* **2013**, *49*, 4896–4898; c) M. A. Wright, J. A. Wright, *Dalton Trans.* **2016**, *45*, 6801–6811.

[5] J. Marhenke, K. Trevino, C. Works, *Coord. Chem. Rev.* **2016**, *306*, 533–543.

[6] a) I. Chakraborty, S. J. Carrington, P. K. Mascharak, *Acc. Chem. Res.* **2014**, *47*, 2603–2611; b) M. Popova, T. Soboleva, S. Ayad, A. D. Benninghoff, L. M. Berreau, *J. Am. Chem. Soc.* **2018**, *140*, 9721–9729; c) T. Soboleva, H. J. Esquer, S. N. Anderson, L. M. Berreau, A. D. Benninghoff, *ACS Chem. Biol.* **2018**, *13*, 2220–2228.

[7] a) A. E. Pierri, A. Pallaoro, G. Wu, P. C. Ford, *J. Am. Chem. Soc.* **2012**, *134*, 18197–18200; b) S. J. Carrington, I. Chakraborty, J. M. L. Bernard, P. K. Mascharak, *ACS Med. Chem. Lett.* **2014**, *5*, 1324–1328; c) L. Wu, X. Cai, H. Zhu, J. Li, D. Shi, D. Su, D. Yue, Z. Gu, *Adv. Funct. Mater.* **2018**, *28*, 1804324; d) E. Kottelat, V. Chabert, A. Crochet, K. M. Fromm, F. Zobi, *Eur. J. Inorg. Chem.* **2015**, *2015*, 5628–5638.

[8] a) C. Bischof, T. Joshi, A. Dimri, L. Spiccia, U. Schatzschneider, *Inorg. Chem.* **2013**, *52*, 9297–9308; b) M. A. Gonzalez, S. J. Carrington, I. Chakraborty, M. M. Olmstead, P. K. Mascharak, *Inorg. Chem.* **2013**, *52*, 11320–11331; c) P. Wang, H. Liu, Q. Zhao, Y. Chen, B. Liu, B. Zhang, Q. Zheng, *Eur. J. Med. Chem.* **2014**, *74*, 199–215; d) J. Jimenez, I. Chakraborty, P. Mascharak, *Acta Crystallogr. Sect. C, Struct. Chem.* **2015**, *71*, 965–968; e) S. Yang, M. Chen, L. Zhou, G. Zhang, Z. Gao, W. Zhang, *Dalton Trans.* **2016**, *45*, 3727–3733; f) M. Kubeil, R. R. Vernooij, C. Kubeil, B. R. Wood, B. Graham, H. Stephan, L. Spiccia, *Inorg. Chem.* **2017**, *56*, 5941–5952; g) N. Pontillo, G. Ferraro, L. Messori, G. Tamasi, A. Merlino, *Dalton Trans.* **2017**, *46*, 9621–9629; h) A. M. Mansour, *Eur. J. Inorg. Chem.* **2018**, *2018*, 852–860; i) M. Chaves-Ferreira, I. S. Albuquerque, D. Matak-Vinkovic, A. C. Coelho, S. M. Carvalho, L. M. Saraiva, C. C. Romão, G. J. L. Bernardes, *Angew. Chem. Int. Ed.* **2015**, *54*, 1172–1175; *Angew. Chem.* **2015**, *127*, 1188–1191; j) A. M. Mansour, *Appl. Organomet. Chem.* **2017**, *31*, e3564.

[9] F. Battistin, D. Siegmund, G. Balducci, E. Alessio, N. Metzler-Nolte, *Dalton Trans.* **2019**, *48*, 400–414.

[10] I. Marin, C. Turta, A. C. Benniston, R. W. Harrington, W. Clegg, *Eur. J. Inorg. Chem.* **2015**, 786–793.

[11] N. L. Fry, P. K. Mascharak, *Acc. Chem. Res.* **2011**, *44*, 289–298.

[12] E. Largy, F. Hamon, F. Rosu, V. Gabelica, E. De Pauw, A. Guédin, J.-L. Mergny, M.-P. Teulade-Fichou, *Chem. Eur. J.* **2011**, *17*, 13274–13283.

[13] a) P. A. Anderson, G. B. Deacon, K. H. Haarmann, F. R. Keene, T. J. Meyer, D. A. Reitsma, B. W. Skelton, G. F. Strouse, N. C. Thomas, J. A. Treadway, A. H. White, *Inorg. Chem.* **1995**, *34*, 6145–6157; b) C. Bischof, T. Joshi, A. Dimri, L. Spiccia, U. Schatzschneider, *Inorg. Chem.* **2013**, *52*, 9297–9308.

[14] I. Krossing, I. Raabe, *Angew. Chem. Int. Ed.* **2004**, *43*, 2066–2090; *Angew. Chem.* **2004**, *116*, 2116–2142.

[15] M. Haukka, P. Hirva, S. Luukkanen, M. Kallinen, M. Ahlgren, T. A. Pakkanen, *Inorg. Chem.* **1999**, *38*, 3182–3189.

[16] A. M. Mansour, O. R. Shehab, *J. Photochem. Photobiol. A* **2018**, *364*, 406–414.

[17] D. H. Gibson, B. A. Sleadd, M. S. Mashuta, J. F. Richardson, *Organometallics* **1997**, *16*, 4421–4427.

[18] a) H. Shaw, S. Toby, *J. Chem. Educ.* **1966**, *43*, 408; b) S. Toby, *J. Chem. Educ.* **2005**, *82*, 37–37.

[19] a) *SHELXS97: Program for Crystal Structure solution*„ University of Göttingen: Göttingen, Germany, **1997**; b) *SHELXL97: Program for Crystal Structure Refinement*, University of Göttingen: Göttingen, Germany, **1997**.

[20] J. Jaumot, R. Gargallo, A. de Juan, R. Tauler, *Chemom. Intell. Lab. Syst.* **2005**, *76*, 101–110.

[21] R. Tauler, A. Smilde, B. Kowalski, *J. Chemom.* **1995**, *9*, 31–58.

Manuscript received: March 27, 2019
Revised manuscript received: May 3, 2019